Electronic Supplementary Material (ESI) for Nanoscale.
This journal is © The Royal Society of Chemistry 2014

Supplementary Information

Carbon Dioxide Conversion into Hydrocarbon Fuels on Defective Graphene-Supported Cu Nanoparticles from First Principles

Dong-Hee Lim1)*, Jun Ho Jo1), Dong Yun Shin1), Jennifer Wilcox2)
Hyung Chul Ham1), and Suk Woo Nam1)

1) Fuel Cell Research Center, Korea Institute of Science and Technology (KIST),
Hwarangno 14-gil 5, Seongbuk-gu, Seoul 136-791, Republic of Korea

2) Department of Energy Resources Engineering, Stanford University
367 Panama Street, Green Earth Sciences, Stanford, CA 94305-2220, USA

* Corresponding author: Dong-Hee Lim
Email: limkr@kist.re.kr, Phone: +82-2-958-5293, Fax: +82-2-958-5199

Journal Name: *Nanoscale*

Author Email Addresses:
Dong-Hee Lim (limkr@kist.re.kr), Jun Ho Jo (galer821@gmail.com),
Dong Yun Shin (84sindy@gmail.com), Jennifer Wilcox (wilcoxj@stanford.edu),
Hyung Chul Ham (hchahm@kist.re.kr), and Suk Woo Nam (swn@kist.re.kr)

1. DFT calculations

Density functional theory calculations were performed using the Vienna *ab initio* Simulation Package (VASP)[1-4] with the projector-augmented wave (PAW)[5,6] method. Electron exchange-correlation functionals were represented with the generalized gradient approximation (GGA), and the model of Perdew, Burke and Ernzerhof (PBE)[7] was used for the nonlocal corrections. A kinetic energy cutoff of 400 eV was used with a plane-wave basis set. The integration of the Brillouin zone was conducted using a 2 × 2 × 1 Monkhorst-Pack grid[8] with the Γ-point included and first-order Methfessel-Paxton smearing[9] with a width of 0.1 eV. The geometries were optimized until the forces were reduced below 10^{-2} eV/Å. Spin polarization was not incorporated since copper is non-magnetic. The spin polarization calculation lowers the free energy barrier up to 0.05 eV between the CO* and CHO* steps on both systems, but does not significantly change the relative energy profiles.

The Cu(111)–*p*(4×4) surface (rhombus-shaped) with a side length of 10.29 Å and an orthorhombic supercell of 14.81 × 12.82 × 24.00 Å were used for the Cu(111) surface and the Cu_{55}–graphene system, respectively. The vacuum space for the systems is larger than 13.80 Å. The Cu(111)–*p*(4×4) surface was represented as a four-layer slab with 16 atoms in each layer where the two bottom layers were fixed at the equilibrium lattice constant of 3.637 Å (experimental measurement 3.615 Å)[10]. The Cu_{55}–graphene system consists of 70 carbon atoms with a 5–8–5 vacancy site of graphene and an icosahedral Cu_{55} cluster. Fully relaxed and optimized Cu_{55}–defective graphene systems were partially frozen for the current study to save computational effort. The boundary 46 carbon atoms out of 70 carbon atoms of defective graphene were frozen based on their negligible influence on the geometry change as shown in our previous study[11].

The isolated Cu_{55} nanoparticle and gas-phase molecules were optimized in a 25.0 and 12.0 Å cubic supercell in which the Brillouin zone integration was carried out for the Γ-point only. The gas-phase molecules were calculated by using a Fermi-level smearing of 0.01 eV, while the isolated Cu_{55} nanoparticle was performed using the same input parameters as described for the surface systems. The adsorption energy (E_{ads}) of an adsorbate is defined as $E_{ads} = E_{substrate+adsorbate} - E_{substrate} - E_{adsorbate}$, where $E_{substrate+adsorbate}$, $E_{substrate}$, and $E_{adsorbate}$ are the total energies of a substrate and adsorbate (e.g., Cu_{55}–defective graphene), a substrate (defective graphene), and a gas phase adsorbate (e.g., Cu_{55}). A negative adsorption energy indicates that adsorption is exothermic (stable) with respect to the free gas-phase adsorbate.

The free energies of the CO_2 reduction intermediates in electrochemical reaction pathways were calculated based on a computational hydrogen electrode (CHE) model suggested by Nørskov *et al.*[12-14] The CHE model defines that the chemical potential of a proton/electron ($H^+ + e^-$) in solution is equal to half of the chemical potential of a gas-phase H_2. The free energy change (ΔG) is calculated as $\Delta G = \Delta E + \Delta ZPE - T\Delta S$, where ΔE is the total energy change directly obtained from DFT calculations, ΔZPE is the change in zero-point energies, T is temperature (18.5 °C), and ΔS is the change in entropy. The free energies of adsorbates were calculated by treating the $3N$ degrees of freedom of the adsorbates as vibrational frequencies in the harmonic oscillator approximation and fixing the Cu_{55}–defective graphene surfaces (assuming the vibrations of the Cu_{55}–defective graphene surfaces are negligible) as done in Peterson *et al.*[14] Zero-point energies and entropies of the CO_2 reduction intermediates were calculated from the vibrational frequencies according to standard methods.[15] The chemical potentials (μ) of the gas-phase molecules were determined by calculating the DFT total energies and ZPE and from the thermodynamics database of Peterson *et al.*[14], as described in Table S1. The solvation energies of adsorbed species are summarized in Table S2. An adsorbate with a negative solvation energy indicates that the adsorbate is stabilized in liquid water by the amount equivalent to the solvation energy.

Table S1. Chemical potentials (μ) of gas-phase molecules obtained by summing up DFT electronic energy (E_{elec}), zero point energy (ZPE), enthalpic temperature correction ($\int C_P dT$), and entropy contribution (–TS). [a] Data from the current study. [b] Data from Peterson *et al.*[14] H_2 (CHE) refers to the gas-phase H_2 used in the CHE model definition.

Species	$E_{elec}{}^{a}$	ZPE^{a} (ZPE^{b})	$\int C_P dT^{b}$	–TS^{b}	μ (eV)	Assumed fugacity (Pa)^{b}
CH_4(g)	-24.03	1.19 (1.20)	0.10	–0.60	-23.34	20,467
CO_2(g)	-22.99	0.28 (0.31)	0.10	–0.65	-23.26	101,325
H_2(g)	-6.76	0.30 (0.27)	0.09	–0.42	-6.79	30,296
H_2O(g)	-14.23	0.60 (0.58)	0.10	–0.65	-14.18	3,534
CO(g)	-14.80	0.12 (0.14)	0.09	–0.67	-15.25	5,562
HCOOH(g)	-29.91	0.86 (0.90)	0.11	–1.02	-29.96	2
H_2 (CHE)	-6.76	0.30 (0.27)	0.09	–0.39	-6.76	101,325

Table S2. Solvation energies (E_{solv}) of adsorbed species obtained from Peterson *et al.*[14]

Adsorbed species	E_{solv} (eV)^{b}
COOH*	–0.25
CO*	–0.1
CHO*	–0.1
CH_2O*	0
CH_3O*	0
O*	0
OH*	–0.5

2. CO_2 reduction pathways on Cu(111) and Cu_{55}–graphene

Table S3. CO_2 reduction reactions and the relative free energies of the CO_2 reduction intermediates on the Cu(111) surface and the Cu_{55}–defective graphene structure used for Figure 2 of the main paper.

Reaction between ($H^+ + e^-$) transfer steps		Relative free energy (eV)			
		Cu(111)		Cu_{55}–graphene	
		$U = 0$	$U = -0.97$	$U = 0$	$U = -0.68$
8→0	$2H_2O + CH_4 + * \rightarrow CO_2 + * + 8H$	1.39	9.18	1.39	6.84
8→1	$2H_2O + CH_4 + * \rightarrow COOH* + 7H$	1.90	8.72	1.59	6.35
8→2	$2H_2O + CH_4 + * \rightarrow CO* + 6H + H_2O$	1.20	7.04	1.29	5.37
8→3	$2H_2O + CH_4 + * \rightarrow CHO* + 5H + H_2O$	2.17	7.04	1.97	5.37
8→4	$2H_2O + CH_4 + * \rightarrow CH_2O* + 4H + H_2O$	2.12	6.01	1.91	4.63
8→5	$2H_2O + CH_4 + * \rightarrow CH_3O* + 3H + H_2O$	1.31	4.24	1.18	3.22
8→6	$2H_2O + CH_4 + * \rightarrow O* + 2H + H_2O + CH_4$	0.66	2.61	0.20	1.56
8→7	$2H_2O + CH_4 + * \rightarrow OH* + H + H_2O + CH_4$	−0.39	0.59	−0.60	0.08
8→8	$2H_2O + CH_4 + * \rightarrow 2H_2O + CH_4 + *$	0.00	0.00	0.00	0.00

3. Projected density of states (PDOS)

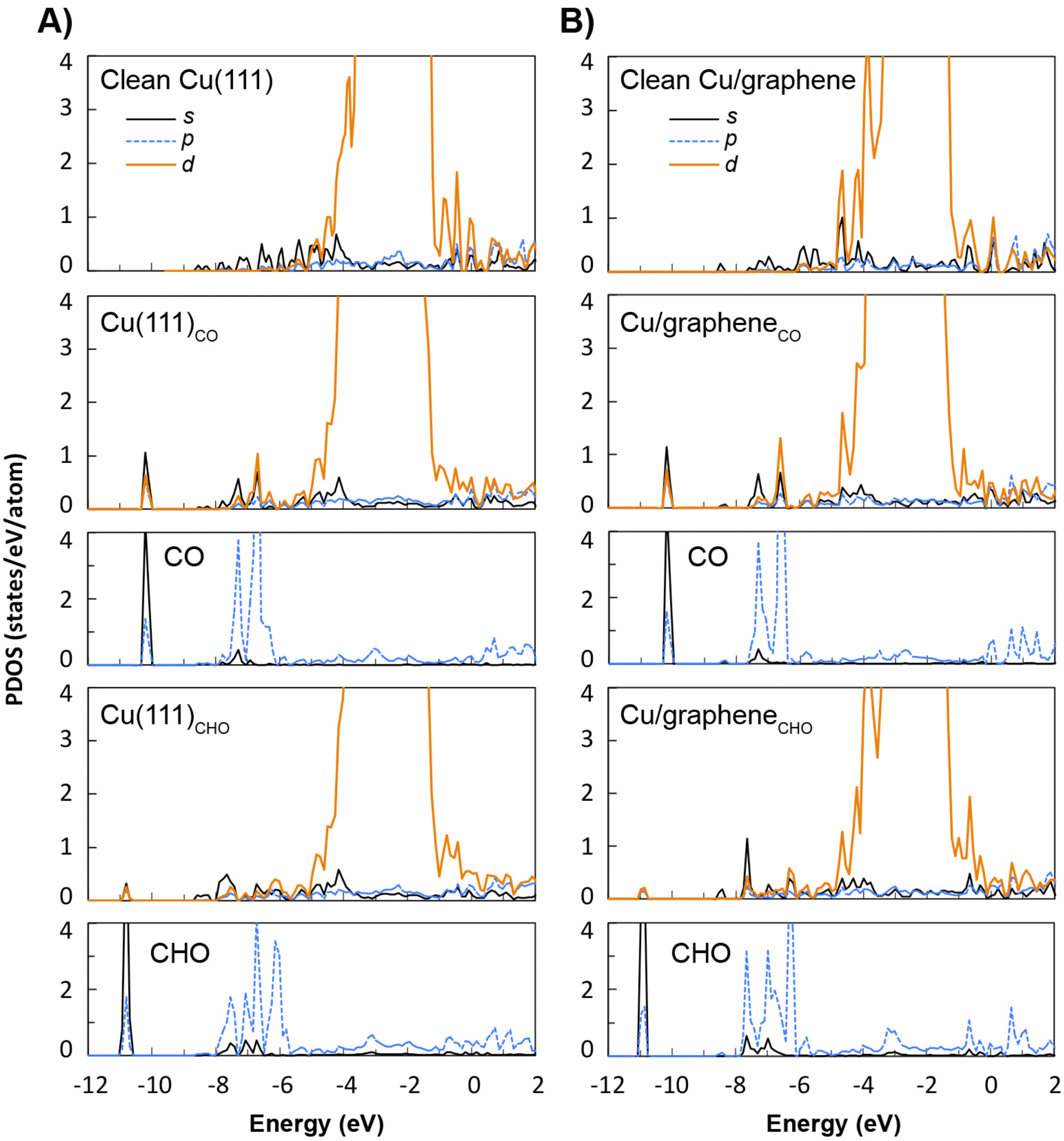

Figure S1. Projected density of states (PDOS) of the Cu(111) (A) and the Cu_{55}-graphene (B) surfaces with adsorbed CO and CHO. A system title of X_Y indicates a surface (X) with adsorbed species (Y). Clean, CO, and CHO represent clean surface without adsorbates, adsorbed CO, and adsorbed CHO, respectively. The Fermi energy is referenced at 0 eV.

4. CHO adsorption configuration on Cu(111) and Cu_{55}–defective graphene

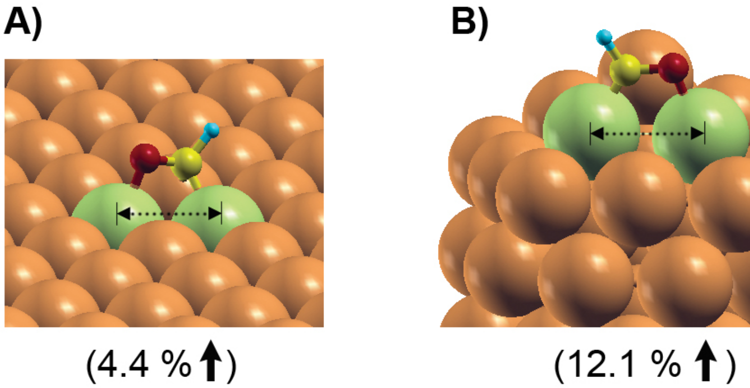

Figure S2. Comparison of Cu–Cu bond distances between the Cu(111) surface and the Cu_{55}–defective graphene system when CHO species is adsorbed. Two different colored Cu atoms on each surface indicate the Cu–Cu distance measured upon adsorption. Numbers with an arrow indicate percentages of enlarged Cu–Cu distances upon CHO adsorption.

5. Solvation effect

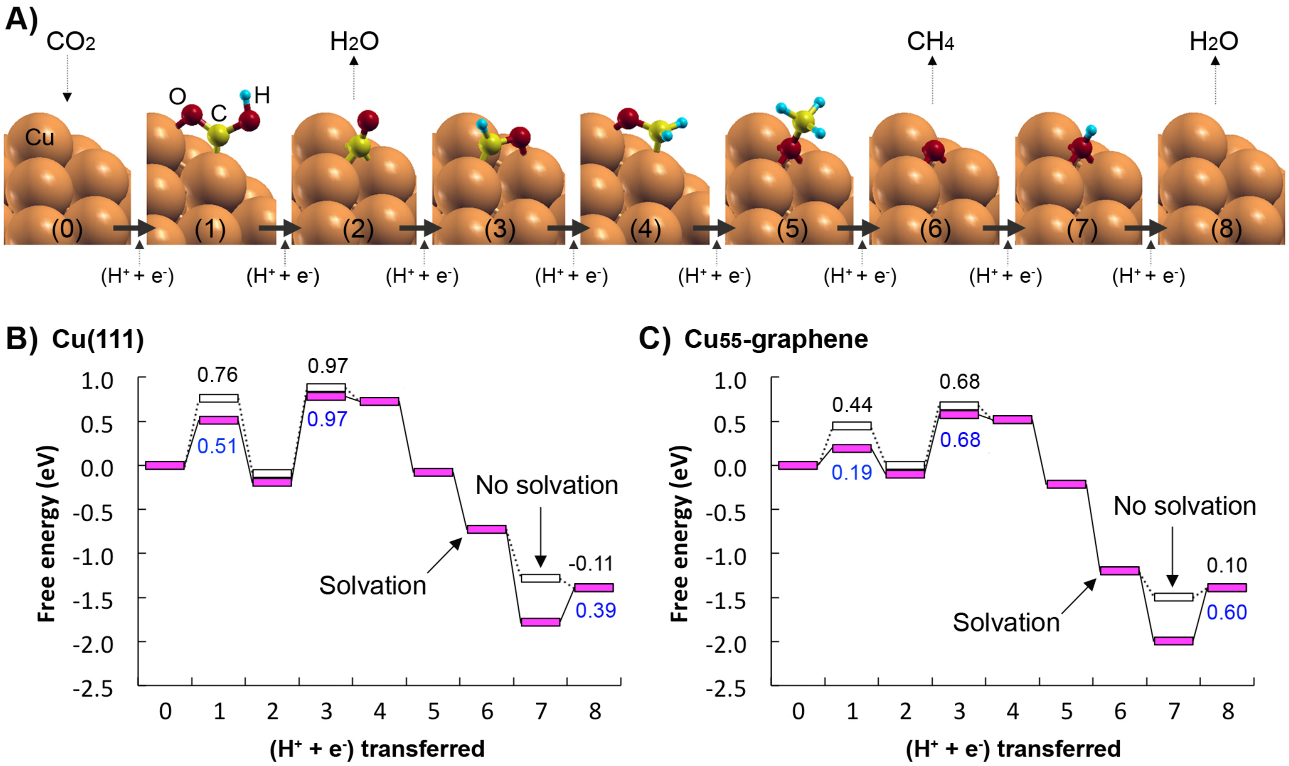

Figure S3. (A) The lowest energy pathways of CO_2 reduction on the Cu_{55}–defective graphene. (B and C) Relative free energy diagrams for CO_2 reduction on Cu(111) and Cu_{55}–defective graphene, respectively with no solvation (empty rectangle with dashed lines) and solvation (filled rectangle with solid lines) consideration.

References

(1) Kresse, G.; Hafner, J., Ab initio molecular dynamics for liquid metals. *Physical Review B* **1993,** *47*, (1), 558-561.

(2) Kresse, G.; Hafner, J., Ab initio molecular-dynamics simulation of the liquid-metal amorphous-semiconductor transition in germanium. *Physical Review B* **1994,** *49*, (20), 14251-14269.

(3) Kresse, G.; Furthmüller, J., Efficient iterative schemes for ab initio total-energy calculations using a plane-wave basis set. *Physical Review B* **1996,** *54*, (16), 11169-11186.

(4) Kresse, G.; Furthmüller, J., Efficiency of ab-initio total energy calculations for metals and semiconductors using a plane-wave basis set. *Computational Materials Science* **1996,** *6*, (1), 15-50.

(5) Blöchl, P. E., Projector augmented-wave method. *Physical Review B* **1994,** *50*, (24), 17953-17979.

(6) Kresse, G.; Joubert, D., From ultrasoft pseudopotentials to the projector augmented-wave method. *Physical Review B* **1999,** *59*, (3), 1758-1775.

(7) Perdew, J. P.; Burke, K.; Ernzerhof, M., Generalized gradient approximation made simple. *Physical Review Letters* **1996,** *77*, (18), 3865-3868.

(8) Monkhorst, H. J.; Pack, J. D., Special points for Brillouin-zone integrations. *Physical Review B* **1976,** *13*, (12), 5188-5192.

(9) Methfessel, M.; Paxton, A. T., High-precision sampling for Brillouin-zone integration in metals. *Physical Review B* **1989,** *40*, (6), 3616-3621.

(10) Straumanis, M. E.; Yu, L. S., Lattice Parameters, Densities, Expansion Coefficients and Perfection of Structure of Cu and of Cu-In alpha Phase. *Acta Crystallographica* **1969,** *A25*, 676-682.

(11) Lim, D. H.; Wilcox, J., Mechanisms of the Oxygen Reduction Reaction on Defective Graphene-Supported Pt Nanoparticles from First-Principles. *Journal of Physical Chemistry C* **2012,** *116*, (5), 3653-3660.

(12) Nørskov, J. K.; Rossmeisl, J.; Logadottir, A.; Lindqvist, L.; Kitchin, J. R.; Bligaard, T.; Jónsson, H., Origin of the overpotential for oxygen reduction at a fuel-cell cathode. *Journal of Physical Chemistry B* **2004,** *108*, (46), 17886-17892.

(13) Rossmeisl, J.; Logadottir, A.; Nørskov, J. K., Electrolysis of water on (oxidized) metal surfaces. *Chemical Physics* **2005,** *319*, (1-3), 178-184.

(14) Peterson, A. A.; Abild-Pedersen, F.; Studt, F.; Rossmeisl, J.; Nørskov, J. K., How copper catalyzes the electroreduction of carbon dioxide into hydrocarbon fuels. *Energy & Environmental Science* **2010,** *3*, (9), 1311-1315.

(15) Cramer, C. J., *Essentials of Computational Chemistry Theories and Models*. 2nd ed.; John Wiley & Sons, Ltd.: West Sussex, England, 2004; p 355-366.